Application Note 44

Terahertz Spectrometer based on Generation of Ultrafast Terahertz Pulses in Air Plasma

Technology and Applications Center
Newport Corporation

Spectra-Physics
A Newport Corporation Brand

Newport
Experience | Solutions

Introduction:

Terahertz (THz) radiation, generally considered as electric fields with wavelengths (frequencies) ranging from 30 µm to 3 mm (0.1 to 10 THz), has attracted great attention in the past two decades[1]. In terms of spectroscopy, specific molecular absorptions in the THz region can be utilized in a wide range of applications from probing crystalline structures[2,3] and protein interactions[4-6], to discerning traces of explosives[7]. A particular strength of THz spectroscopy is that it provides a non-invasive tool to help in understanding physical science. In terms of imaging[8], the ability to penetrate optically opaque materials, such as plastics, clothing, and biological tissues, makes it useful for applications including 2D and/or 3D medical imaging[9], pharmaceutical sciences[3], and security screening[10]. With all these fields burgeoning, novel and neat experimental designs for THz generation are essential to complement the development of THz research.

In this note, we focus on the generation of THz pulses (~1 ps) in air plasma. While it is already popular to generate THz pulses using biased photoconductive antennas[11], advancements in laser amplifiers offer a new methodology based on air plasma generation. Pioneered by Hamster, Sullivan and coworkers with unbiased air plasma in 1993[12], and by Cook and Hochstrasser with AC-biased air plasma in 2000[13], further adoption of this method has taken place due to several advantages, including straightforward implementation of the setup, practically no damage threshold of the ambient air, and strong field strength comparable with antenna-based generation[14,15]. In this note, we basically follow the work done by Cook and Hochstrasser to demonstrate the feasibility of THz generation based on a sub-35 fs, 800 nm ultrafast laser amplifier.

In brief, the 800 nm laser pulse (1 kHz, ~ 300 µJ per pulse) is focused into ambient air to generate the air plasma. Right before the focal point, a BBO crystal is inserted to create second harmonic generated (SHG) 400 nm, converted from the 800 nm fundamental. The oscillating 400 nm field acts as AC-bias at the focal point to polarize the plasma by drifting the electrons away from the nuclei. This process, combined with the re-collision of the electrons collapsing toward the nuclei, creates a transient current and as a result, a strong THz field is generated. This highly nonlinear process makes the efficiency of the THz generation sensitive to the carrier envelope phase (CEP) of the ultrafast laser pulses and it has been demonstrated that this effect can be used to monitor and stabilize the CEP of a laser amplifier system[16].

The detection of the THz field utilizes electro-optic sampling with the help of a ZnTe crystal. By mixing the THz field and the 800 nm probe in the ZnTe crystal, the time domain trace of the THz amplitude is recovered directly from the signal (intensity difference) from a balance detector[17]. In addition, it is straightforward to measure the absorption spectra of the materials by putting them into the beam path without changing the setup, which means we also have a THz spectrometer. In this note, we will demonstrate this feature by measuring the absorption of water vapor in the THz region.

Experimental setup

The layout of the setup is shown in figure 1. The output of the Spectra-Physics Spitfire® Pro XP ultrafast amplifier is split (see ***Multimodal Ultrafast Spectroscopy System Based on a 35 Femtosecond Ti:Sapphire Chirped Pulse Amplification (CPA) Laser - application note 41*** for a recommendation on how to split the beams), such that a portion of the output (~300 µJ, P-polarized) is used for the experiment.

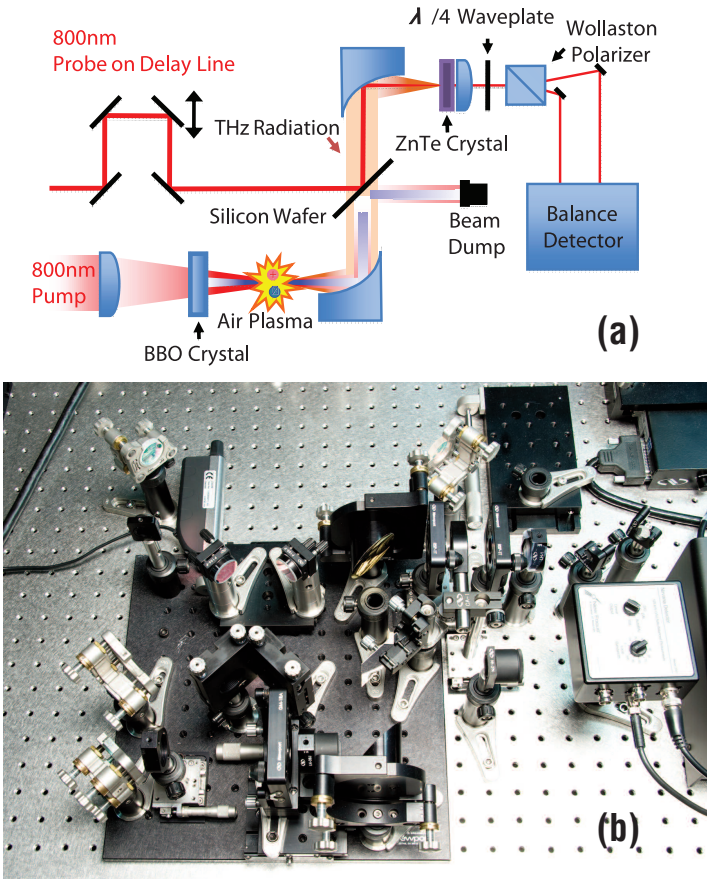

Figure 1. The experimental layout of the setup. (a) The schematic presentation. (b) The working setup in Newport's Technology and Applications Center.

Initially, the energy of the laser pulse is reduced to about 10 µJ (by use of a variable neutral density filter before mirror $\mathbf{M}_1$, not shown). Then, as shown in Figure 2(a), mirrors $\mathbf{M}_1$ and $\mathbf{M}_2$ are used to align the laser pulse parallel to the table and the side of the breadboard. The laser pulse should be kept parallel to the table at all times (5 inches in this setup). This minimizes the aberration caused by other optics in the beam path. An iris ($\mathbf{I}_1$) is used to help meet this requirement. Subsequently, a beam sampler ($\mathbf{BS}_1$) is installed at a 45° angle to the incoming beam passing through its center. The beam sampler reflects 3% of the energy for use as the probe beam.

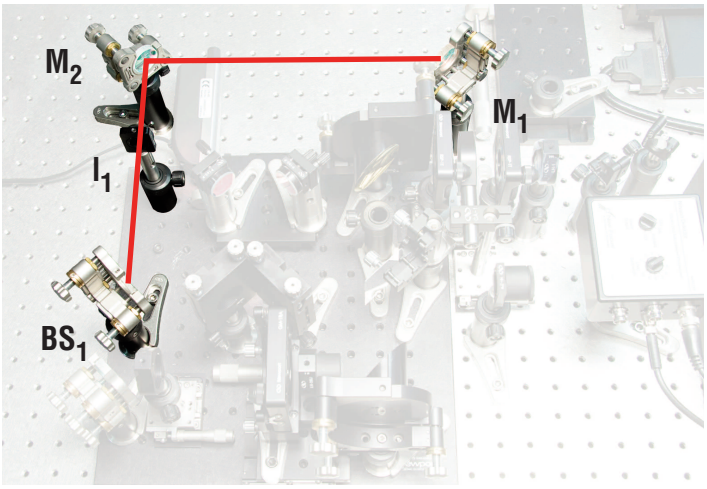

Figure 2(a). Alignment of the beam into the setup.

The pump beam (the pulse train that transmits through **BS**$_1$) is folded 90° by **M**$_3$ such that it travels parallel to the side of the breadboard (Figure 2(b)). A lens (**L**$_1$) with 125 mm focal length, mounted on a translational stage (**TS**$_1$), is positioned in a way that the pump beam passes through its center.

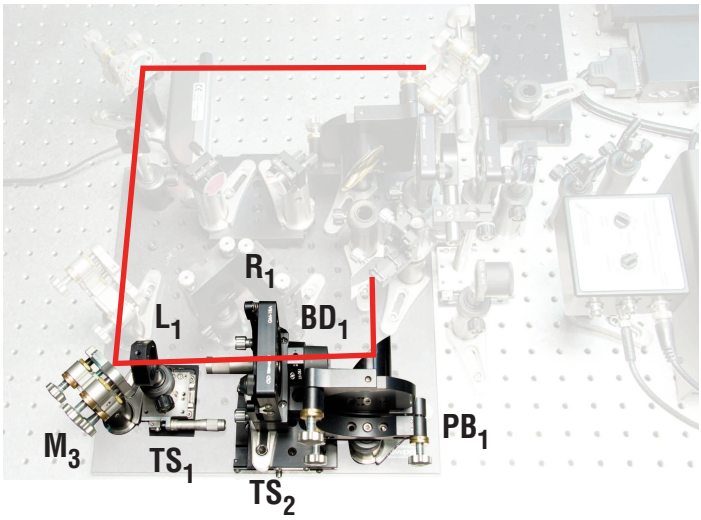

Figure 2(b). Alignment of the pump beam to generate air plasma.

A 100 µm thick type I BBO crystal mounted in a rotational stage (**R**$_1$), and on a linear stage (**TS**$_2$) is placed after the lens (**L**$_1$). This assembly is positioned normal to the beam path, with the BBO crystal about 25 mm prior to the focal point, and used to generate 400 nm. The BBO crystal is rotated to the optimum angle for efficient generation of 400 nm. It is then detuned from this position by adjusting **R**$_1$ (~ 35°) to create enough 400 nm with the same polarization as the fundamental. This adjustment will be fine-tuned later for the optimization of the THz field. The power is increased by rotating the neutral density filter such that air plasma is just observed at the focal point. A beam dump (**BD**$_1$) with the back plate removed is then mounted on **TS**$_2$ to prevent the strong white light from reaching the eyes. Reduce the power back to 10 µJ after **BD**$_1$ is set.

A parabola (**PB**$_1$, 50 mm EFL) is positioned about 50 mm away from the focal point such that the pulse is folded 90° and travels along the side of the breadboard and parallel to the table. **TS**$_1$ is adjusted such that the beam after the parabola is collimated.

The probe beam is routed by **M**$_4$ to a retro-reflector consisting of **M**$_5$ and **M**$_6$ (figure 2(c)). This retro-reflector is mounted on a motorized delay stage (**MS**$_1$) for the purpose of controlling the electro-optic sampling. The probe beam is then redirected by **M**$_7$. Initially, each mirror, from **M**$_4$ to **M**$_7$, will fold the probe beam exactly 90°. When inserting a business card into the probe beam bouncing off **M**$_7$ and adjusting **MS**$_1$, no displacement of the probe beam should be observed on the business card. Adjusting **M**$_4$ may be necessary so that the probe beam does not walk on **M**$_5$ when **MS**$_1$ is translated. Subsequently, mirrors **M**$_5$ and **M**$_6$ are adjusted such that the probe beam remains centered on **M**$_7$ when **MS**$_1$ is translated. Also, the distance the probe travels from **BS**$_1$ to flip mount **S** (figure 2(d)) needs to closely match that traveled by the pump from **BS**$_1$ to **S**.

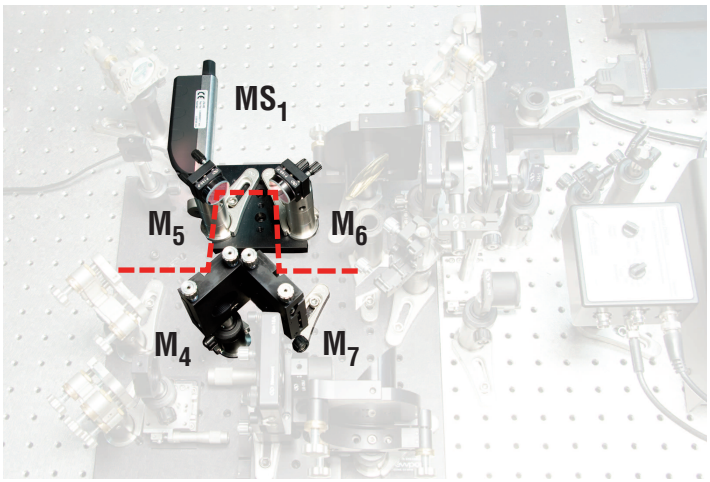

Figure 2(c). Alignment of the probe beam.

At this point, the setup is prepared for recombining pump and probe beams. The beam path of the pump will be used as a guide for that of the THz beam generated when the pump power is increased later on. The silicon wafer (400 µm thick, both sides polished) is on a flip mount (**S**) and used as a combining mirror. It is also utilized to filter out and dump 400 nm, 800 nm, and strong white light generated (figure 2(d)).

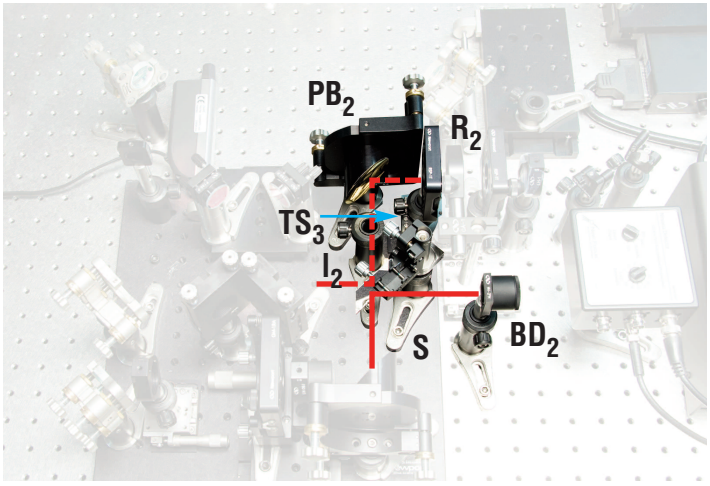

Figure 2(d). Recombination of the probe beam with THz field.

The flip mount **S** is set that the pump beam is allowed to hit the center of the parabola $\mathbf{PB}_2$ and folded 90°. After inserting an iris ($\mathbf{I}_2$) between $\mathbf{PB}_2$ and **S**, it is positioned so that the pump beam passes through its center. The <110> ZnTe crystal on the rotational stage $\mathbf{R}_2$ is positioned normal to the pump beam and at the focus of $\mathbf{PB}_2$. $\mathbf{R}_2$ is on a translation stage ($\mathbf{TS}_3$), which is used for fine positioning. The pump beam should hit and focus onto the center of the crystal. The pump beam power may need to be attenuated to prevent any damage to the crystal. The mount (**S**) is flipped to its original position (it should be 45° to either pump or probe beam at this position). Beam dump ($\mathbf{BD}_2$) captures the rejected pump beam. Mirror $\mathbf{M}_7$ is used to center the probe through $\mathbf{I}_2$, and subsequently **S** is adjusted such that the probe beam hits the center of the ZnTe crystal. Some iteration is required.

After the above procedure, a lens with 25 mm focal length ($\mathbf{L}_2$) on a delay stage ($\mathbf{TS}_4$) is inserted right after $\mathbf{R}_2$ to collimate the probe beam (figure 2(e)). $\mathbf{TS}_4$ is adjusted for the probe beam to be collimated. The collimated probe beam is then sent through a quarter-wave plate (**QW**) and a Wollaston polarizer (**WP**) to create two beams with perpendicular polarizations. **QW** is rotated such that the two beams exiting **WP** have the same intensity.

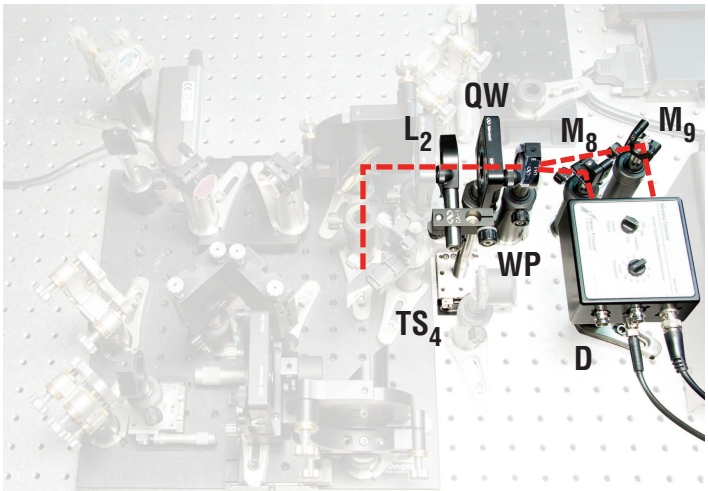

Figure 2(e). Sending the probe beam into the balance detector for electro-optic sampling.

After routing the beams to the entrance ports of the ***balance detector*** (**D**) using mirrors $\mathbf{M}_8$ and $\mathbf{M}_9$, respectively, a co-axial cable is connected from the differential output of the balance detector to an oscilloscope. At this point, the balance detector should indicate null response since the intensities of the two beams should be equal. If not, rotate **QW** such that a null response is achieved. Increasing the pump energy to around 150 μJ will generate air plasma. At this point, when the delay is adjusted using $\mathbf{MS}_1$ within its full range, and the timing is right, you will see the signal (intensity difference, figure 3) is oscillating between negative and positive. This is caused by the THz that is generated from the air plasma.

The distance between the BBO crystal and the air plasma determines the phase relationship between SHG and the fundamental. Changing the distance between them directly relates to how far the 400 nm can drift away the electrons, which relates to how strong the THz will be as the electrons recombine. So, once the THz signal is observed, it can be optimized by adjusting $\mathbf{TS}_2$ and $\mathbf{R}_1$ (the "detune angle"). Tweaking **S** for better spatial overlap between the probe and THz beams may also improve the signal. After any of these steps, adjusting $\mathbf{MS}_1$ will be required for the optimization of the THz signal.

Results

The generated THz field is shown in figure 3. Several features can be observed in the time domain trace. First of all, the main oscillation is only one cycle and spans about 1 ps. It contains most of the THz energy, and is estimated to be about 0.1-0.3 nJ per pulse[14]. Secondly, small and complicated oscillations after the main cycle are observed which indicate something absorbs the THz while it is propagating in air. Thirdly, there is a second, smaller peak around 11.5 ps as shown in figure 3(a). This is actually resulting from the second reflection of the THz within the Silicon wafer. Since it is about 0.4 mm in thickness and it has $n \sim 3.4$ in the THz region, it would cause the delay that is observed in the plot.

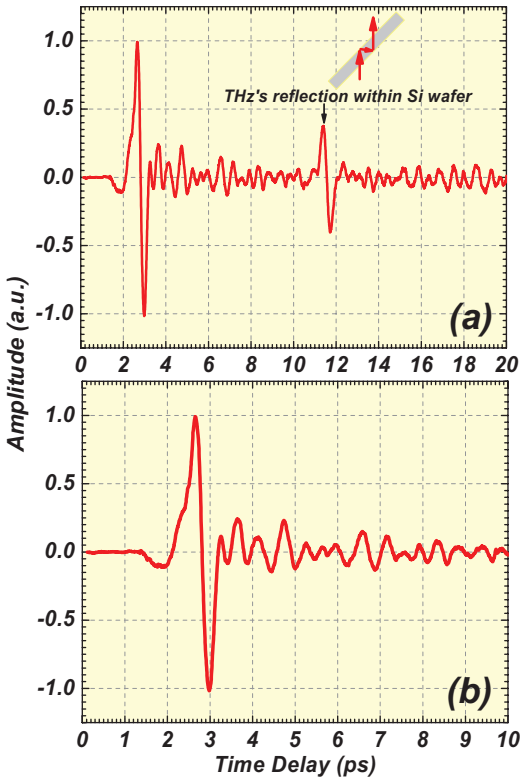

Figure 3. The time trace of THz field collected by electro-optic sampling. (a) The time trace of the first 20 ps of the THz field. (b) Zoomed view of the first 10 ps shows the main cycle and the small complicated oscillations that follow.

The time domain trace is Fourier transformed to show the frequency spectrum of the THz radiation (figure 4). The spectrum spans from 0 to 3 THz. Some sharp absorption lines corresponding to the complicated oscillations after the main cycle are clearly resolved. These are the absorption lines of water vapor's rotational transitions [18,19]. This demonstrates that the setup is actually a THz spectrometer. In addition, by purging the system to remove the water vapor absorption and putting samples into the beam path of the THz pulse, we can actually measure the spectra of different molecules in the THz region. A lot of explosives and drugs have strong and unique THz absorptions and this feature makes a THz spectrometer much more valuable in detection and spectroscopic applications[21].

The amplitude of the THz field with respect to the input energy is shown in figure 4(c). By extrapolation, the curve would intersect with the positive x axis which means that a certain amount of input energy is required to overcome some threshold before the THz can be generated. This threshold is the energy required to rip the electrons from the nuclei and corroborates the statement that the generation of the plasma is necessary for the THz generation. On the other hand, at high pulse energies, the defocusing of the laser beam by the plasma becomes important and limits the peak intensity of the laser pulse at the focal point[21]. As a result, the efficiency drops. From our design, it is seen that around 250 μJ input energy is optimal in terms of efficiency and the THz intensity.

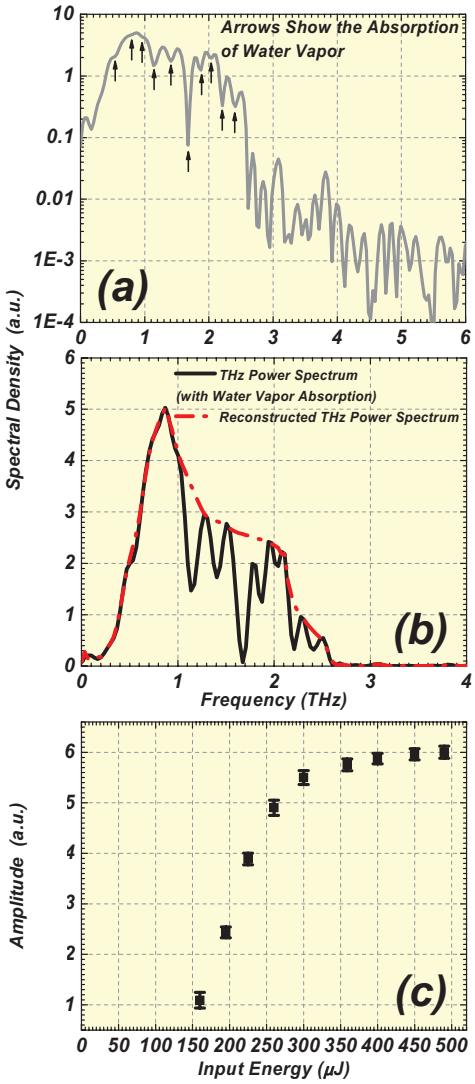

Figure 4. (a) and (b), The spectrum of the generated THz field. (c) The amplitude of the generated THz field is plotted against the input energy.

Conclusion

The setup shows a straightforward implementation of a THz generation tool based on a laser amplifier. The damage threshold is not a concern based on this design and the fact that air plasma generates THz. The strong strength and the pulsed nature of the THz field make it applicable not only to linear spectroscopy in THz domain, but also to time resolved nonlinear experiments, such as optical pump and THz probe experiments. Furthermore, being able to recover the phase and the amplitude information of the THz field through electro-optic sampling adds the functionality of a "THz spectrometer" without further modification.

Newport Corporation

Worldwide Headquarters
1791 Deere Avenue
Irvine, CA 92606

(In U.S.): 800-222-6440
Tel: 949-863-3144
Fax: 949-253-1680

Email: sales@newport.com

Newport
Experience | Solutions

Visit Newport Online at: **www.newport.com**

References:

1. Ferguson, B. and X.C. Zhang, Materials for terahertz science and technology. Nature Materials, 2002. 1(1): p. 26-33.
2. Strachan, C.J., et al., Using terahertz pulsed spectroscopy to quantify pharmaceutical polymorphism and crystallinity. Journal of Pharmaceutical Sciences, 2005. 94(4): p. 837-846.
3. Zeitler, J.A., et al., Terahertz pulsed spectroscopy and imaging in the pharmaceutical setting - a review. Journal of Pharmacy and Pharmacology, 2007. 59(2): p. 209-223.
4. Ebbinghaus, S., et al., An extended dynamical hydration shell around proteins. Proceedings of the National Academy of Sciences of the United States of America, 2007. 104(52): p. 20749-20752.
5. Plusquellic, D.F., et al., Applications of terahertz spectroscopy in biosystems. Chemphyschem, 2007. 8(17): p. 2412-2431.
6. Xu, J., K.W. Plaxco, and S.J. Allen, Probing the collective vibrational dynamics of a protein in liquid water by terahertz absorption spectroscopy. Protein Science, 2006. 15(5): p. 1175-1181.
7. Shen, Y.C., et al., Detection and identification of explosives using terahertz pulsed spectroscopic imaging. Applied Physics Letters, 2005. 86(24).
8. Chan, W.L., J. Deibel, and D.M. Mittleman, Imaging with terahertz radiation. Reports on Progress in Physics, 2007. 70(8): p. 1325-1379.
9. Wallace, V.P., et al., Three-dimensional imaging of optically opaque materials using nonionizing terahertz radiation. Journal of the Optical Society of America a-Optics Image Science and Vision, 2008. 25(12): p. 3120-3133.
10. Kemp, M.C., et al., Security applications of terahertz technology, in Terahertz for Military and Security Applications, R.J. Hwu and D.L. Woodlard, Editors. 2003. p. 44-52.
11. Tani, M., et al., Emission characteristics of photoconductive antennas based on low-temperature-grown GaAs and semi-insulating GaAs. Applied Optics, 1997. 36(30): p. 7853-7859.
12. Hamster, H., et al., Subpicosecond, electromagnetic pulses from intense laser-plamsa interaction. Physical Review Letters, 1993. 71(17): p. 2725-2728.
13. Cook, D.J. and R.M. Hochstrasser, Intense terahertz pulses by four-wave rectification in air. Optics Letters, 2000. 25(16): p. 1210-1212.
14. Loffler, T., et al., Comparative performance of terahertz emitters in amplifier-laser-based systems. Semiconductor Science and Technology, 2005. 20(7): p. S134-S141.
15. Thomson, M.D., et al., Broadband THz emission from gas plasmas induced by femtosecond optical pulses: From fundamentals to applications. Laser & Photonics Reviews, 2007. 1(4): p. 349-368.
16. Kress, M., et al., Determination of the carrier-envelope phase of few-cycle laser pulses with terahertz-emission spectroscopy. Nature Physics, 2006. 2(5): p. 327-331.
17. Planken, P.C.M., et al., Measurement and calculation of the orientation dependence of terahertz pulse detection in ZnTe. Journal of the Optical Society of America B-Optical Physics, 2001. 18(3): p. 313-317.
18. Xin, X., et al., Terahertz absorption spectrum of para and ortho water vapors at different humidities at room temperature. Journal of Applied Physics, 2006. 100(9).
19. Zhou, Z., et al., Terahertz generation and detection setup based on pump-probe scheme. Microwave and Optical Technology Letters, 2009. 51(7): p. 1617-1619.
20. Mlejnek, M., E.M. Wright, and J.V. Moloney, Femtosecond pulse propagation in argon: A pressure dependence study. Physical Review E, 1998. 58(4): p. 4903-4910.
21. Federici, J.F., et al., THz imaging and sensing for security applications - explosives, weapons and drugs. Semiconductor Science and Technology, 2005. 20(7): p. S266-S280.

This Application Note has been prepared based on development activities and experiments conducted in Newport's Technology and Applications Center and the results associated therewith. Actual results may vary based on laboratory environment and setup conditions, the type and condition of actual components and instruments used and user skills.

Nothing contained in this Application Note shall constitute any representation or warranty by Newport, express or implied, regarding the information contained herein or the products or software described herein. Any and all representations, warranties and obligations of Newport with respect to its products and software shall be as set forth in Newport's terms and conditions of sale in effect at the time of sale or license of such products or software. Newport shall not be liable for any costs, damages and expenses whatsoever (including, without limitation, incidental, special and consequential damages) resulting from any use of or reliance on the information contained herein, whether based on warranty, contract, tort or any other legal theory, and whether or not Newport has been advised of the possibility of such damages.

Newport does not guarantee the availability of any products or software and reserves the right to discontinue or modify its products and software at any time. Users of the products or software described herein should refer to the User's Manual and other documentation accompanying such products or software at the time of sale or license for more detailed information regarding the handling, operation and use of such products or software, including but not limited to important safety precautions.

This Application Note shall not be copied, reproduced, distributed or published, in whole or in part, without the prior written consent of Newport Corporation.

Copyright ©2011 Newport Corporation. All Rights Reserved. Spectra-Physics®, the Spectra-Physics "S" logo, the Newport "N" logo, are registered trademarks of Newport Corporation. Newport™ is a trademarks of Newport Corporation.

Newport Corporation, Irvine, California, has been certified compliant with ISO 9001 by the British Standards Institution.

DS-011107